EXPERIMENTAL AND NUMERICAL INVESTIGATIONS ON GLUED JOINTS FOR WIDE-SPAN TIMBER TRUSSES

EXPERIMENTELLE UND NUMERISCHE UNTERSUCHUNGEN ZU GEKLEBTEN ANSCHLÜSSEN FÜR WEITGESPANNTE HOLZ-FACHWERKTRÄGER

Lisa Stimpfle[1], Cristóbal Tapia[1], Jan L. Wenker[2], Simon Aicher[1]

[1] *Materials Testing Institute (MPA), University of Stuttgart, Otto-Graf-Institute*

[2] *Brüninghoff Group, Heiden*

SUMMARY

It is reported on the load capacity of glued hybrid timber truss joints. The investigated connection detail consists of a twin chord made of glued laminated timber from laminated beech veneer lumber (GLVL) and a longitudinally arranged diagonal member from spruce GLT in-between. The axes and fiber directions of the diagonal and chord components include an angle of 63°. The glued connection detail with a lap shear bond area of 893 cm^2 was tested in full scale in tension shear with 12 specimens in a pull-compression test configuration. The load capacities of the joints manufactured with a general purpose phenol-resorcinol adhesive using six different bonding parameter configurations resulted in a mean value and coefficient of variation (COV) of 255 kN and 10%. The mean and minimum apparent bond shear strength were 1.42 MPa and 1.28 MPa, respectively.

The main focus of the paper consists in the creation and calibration of a non-linear finite element model (FEM), using the FEM code Abaqus for analysis of the joint capacity. The joint was modeled in 3D, considering the adherends as components with linear elastic behavior. The bonded interface was realized by non-linear cohesive contact including a linear energy-based softening. The damage initiation is controlled by a maximum nominal shear stress criterion.

Firstly, the effect of numerical damage stabilization on the maximum capacity and on the descending load path by means of viscous regularization was investigated. Following, a sensitivity analysis and inverse calibration of the test results was performed with the cohesive interface parameters—local shear strength of the adherends and fracture energy. In a third step the damage evolution in the bonded

area was analyzed in the pre-peak and ultimate load state as well as on the descending load path. The localization of the damage on-set in the bond area and the further spacial evolution of damage and related stress shifts were clearly identified in quantitative terms. The results of the ongoing work assist the optimum layout of the geometry and sizes of bonded (hybrid) timber truss joints.

ZUSAMMENFASSUNG

Es wird über die Tragfähigkeit von verklebten hybrid aufgebauten Anschlüssen von Holz-Fachwerkträgern berichtet. Das untersuchte Knotendetail besteht aus einem Doppelgurt aus Brettschichtholz aus Buchenfurnierschichtholz (GLVL) und einer dazwischen befindlichen Diagonale aus Fichten-Brettschichtholz (BSH). Die Bauteile sind unter einem Winkel von 63° bezüglich ihrer Längsachsen und Faserrichtungen miteinander verklebt. Die geklebte Verbindung mit einer Scherklebefläche (einschnittig) von 893 cm^2, wurde anhand von 12 Probekörpern vollmaßstäblich auf Zugscheren in einer Zug-Druck-Prüfanordnung getestet. Die Tragfähigkeiten der Verbindungen, die mit einem fugenfüllenden Phenol-Resorcin-Klebstoff in sechs Konfigurationen mit verschiedenen Verklebungsparametern hergestellt wurden, wiesen einen Mittelwert und einen Variationskoeffizienten von 255 kN und 10% auf. Die mittlere und minimale nominelle Scherfestigkeit der Verbindung betrug 1,42 MPa bzw. 1,28 MPa.

Der Schwerpunkt der Arbeit liegt in der Erstellung und Kalibrierung eines nichtlinearen Finite-Elemente-Modells (FEM) unter Verwendung der Sofware Abaqus zur Analyse des Tragverhaltens der Klebefuge. Der Anschluss wurde in 3D modelliert, wobei für die Fügeteile linear-elastisches Materialverhalten angesetzt wurde. Für das geklebte Interface wurde ein nichtlinear kohäsiver Kontakt mit einer energiebasierten Dehnungsentfestigung angenommen. Die Schädigungsinitiierung wird mittels des Maximalwertes eines Scherfestigkeitskriteriums gesteuert.

In einem ersten Schritt wurde der Einfluss einer numerischen Schädigungsstabilisierung auf den Höchstlastbereich und den absteigenden Lastpfad mittels der im Rechenprogramm implementierten viskosen Regularisierung untersucht. Nachfolgend wurde sodann eine Sensitivitätsanalyse der kohäsiven Interfaceparameter – lokale Fügeteilscherfestigkeiten und Bruchenergie – mit einer inversen Kalibrierung an den Versuchsergebnissen durchgeführt. In einem dritten Schritt wurde die Schädigungsentwicklung in der Klebefläche im Lastbereich unmittelbar vor

und bei Höchstlast, sowie auf dem absteigenden Lastpfad analysiert. Die Lokalisierung des Schädigungsbeginns im Bereich einer geometrischen Unstetigkeit der Klebefläche und die nachfolgende, flächige Entwicklung der Schädigung und der Spannungsverschiebungen wurden quantitativ klar identifiziert. Die Ergebnisse der fortlaufenden Arbeit unterstützen die Optimalauslegung der Geometrie und der Größen der geklebten (hybriden) Holzfachwerkverbindungen.

1. INTRODUCTION

It is undisputed that the use of truss-like systems for free-span structures represents an efficient design in terms of used material and structural stiffness [17] as well as load capacity. This is especially true for wide-span constructions, such as hall-roofs or bridges, where large material savings can be achieved. In the field of timber structures, trusses become competitive for spans beyond about 25–30 m, e.g. [24], and have traditionally been widely used in many applications. Timber, being a highly anisotropic material with its strongest direction co-linear with its fibers, can achieve a high degree of structural utilization in trusses, making a very efficient use of the mechanical properties of the material. However, the connection of the truss components at the truss joints, where the members meet at different angles with respect to the fiber—thus demanding the material in its weak directions—, states the most decisive structural detail of timber trusses. Similar to steel trusses, the joints can be either realized with mechanical fasteners or bonded, representing the quasi equivalent to welding in steel structures.

Mechanical joints for timber trusses come mostly in two types: (i) solutions based on slotted-in steel plates connecting the individual truss members by means of dowel-type fasteners, and (ii) screws and dowels directly connecting the wooden members of the joint. Although the reliability of these connections in terms of strength is undisputed and has benefited from large amounts of experimental data—thus, ensuring a safe design—, the observed degradation of stiffness can present serious problems for the serviceability. The stiffness degradation originates from the local embedment indentations and crushing of the timber material in the periphery of the mechanical fasteners, especially dowel-type fasteners. This phenomenon has a pronounced effect on the global deformations of the structure, being in the long term similarly important as the creep effect. The described behavior of connections with dowel-type fasteners becomes even more aggravated in case of cyclic/fatigue loading, where the repeated change in load direction produces an ovalization pinching of the fastener hole, hence allowing for a contact-free sliding of the dowel-type fastener during the load-reverse.

The mentioned drawbacks of mechanically jointed trusses has been a recognized problem for a long time, and has impulsed research in the development of alternative solutions, e.g. based on bonded connections. The benefit of bonded joints consists in the fact that the connection can be considered rigid for monotonic, cyclic and long-term loading. Therefore, the serviceability is drastically improved compared to mechanical fasteners, which enables a more efficient design, as large-span structures tend to be governed by their maximum deflections.

Several very successful industrial initiatives to develop, manufacture and install bonded connections for joints of timber trusses have been made in the past and some are on-going. A prominent example of bonded trusses were e.g. the so-called DSB-trusses manufactured during 1950-1980 highly customized with heights and lengths up to 1 m and 20 m, respectively [11]. Glued form-work trusses of type L24 according to EN 13377 [6], brand name “GT truss”, are manufactured fully automatized/robotically by company Peri, Weißenhorn, Germany, representing a highly competitive alternative to full-webbed form work beams. Regarding trusses with wide spans up to about 30 m, company Wiehag GmbH, Altheim, Austria, has developed and manifold realized a patented bonded GLT truss, brand name “Freespan”, for arched or double tapered roof systems, where the truss joints are realized by laterally glued-on plates made of laminated veneer lumber.

Experimental and numerical investigations on the load carrying capacity of glued truss joints with adherends bonded at different angles have been presented i.a. by Glos and Horstmann [10]. Fundamental non-linear fracture-mechanics related work on glued wooden lap joints has been contributed by Wernersson [20, 21], Wernersson and Gustafsson [22, 23], Serrano [15], Serrano and Gustafsson [16]. Contributions on different probabilistic aspects and related design of glued wooden (hybrid) lap joints are reported by Aicher and Klöck [3] and Tannert et al. [18]. Test and calculation results on bonded lap and truss joints based on glued-in steel plates are given e.g. in Palm [14], Johansson [12], Aicher [2], Kemmsies [13] and Valleé et al. [19]. Summarizing the presently available theoretical and practical experience concerning glued timber truss joints, it can be stated that the evident potential of glued joints is not exploited, rendering mechanically jointed or contact-based connections the best available option. This situation is the onset for a new attempt on bonded joints for timber trusses.

Recently, the company Brüninghoff Holz GmbH & Co. KG, Heiden, concluded a research project with the RheinMain University of Applied Sciences, aiming at

hybrid timber trusses with bonded connections [5]. The diagonals are made of glued laminated timber (GLT) from spruce and the chords consist of laminated veneer lumber (GLVL) made from beech wood. Within the mentioned project some experimental investigations on full-sized joints were performed at MPA, Department of Timber Constructions, University of Stuttgart, too. In order to further develop concepts of glued trusses a research cooperation between the company Brüninghoff Holz GmbH & Co. KG and the MPA was initiated. The objective of this cooperation, coinciding with similar aims of MPA, Timber Dept., in the University of Stuttgart's Cluster of Excelence IntCDC, consists in the further development of bonded timber truss connections by means of non-linear finite element (FE) modelling and a systematic experimental campaign. This paper presents first results of ongoing work.

2. STUDIED SPECIMEN CONFIGURATION AND EXPERIMENTAL SET-UP

The investigated specimens represent a connection detail of a glued wooden truss composed of a diagonal member jointed in-between two twin chords. The chords are made of glued laminated veneer lumber (GLVL) from beech wood, strength class GL75 [9], while the diagonal arranged between the chords consists of homogeneous built-up glulam made from spruce softwood, strength class GL24h according to DIN EN 14080 [7]. The cross-sectional dimensions (thickness t × height h) of the beech GLVL chords are 120 mm × 240 mm and those of the GLT diagonals are 115 mm × 400 mm. The GLVL members are connected to the GLT member at an angle of 63° with respect to their fiber direction (see Fig. 1). The bonded connection between the chords and the diagonal members is performed with a general purpose phenolic-resorcinol adhesive of type EN 301 I 90 GP 0,6 Mw [8]. The quality and mechanical properties of the bonded connection were investigated for varying bonding-related parameters, specifically air humidity, waiting times and adherend side of adhesive application, in order to asses their influence on the connection capacity. This resulted in six subseries, I to VI, each with two test specimens. The connections were produced by the company Brüninghoff Holz GmbH & Co. KG, Heiden, with a prototype press developed for this specific purpose.

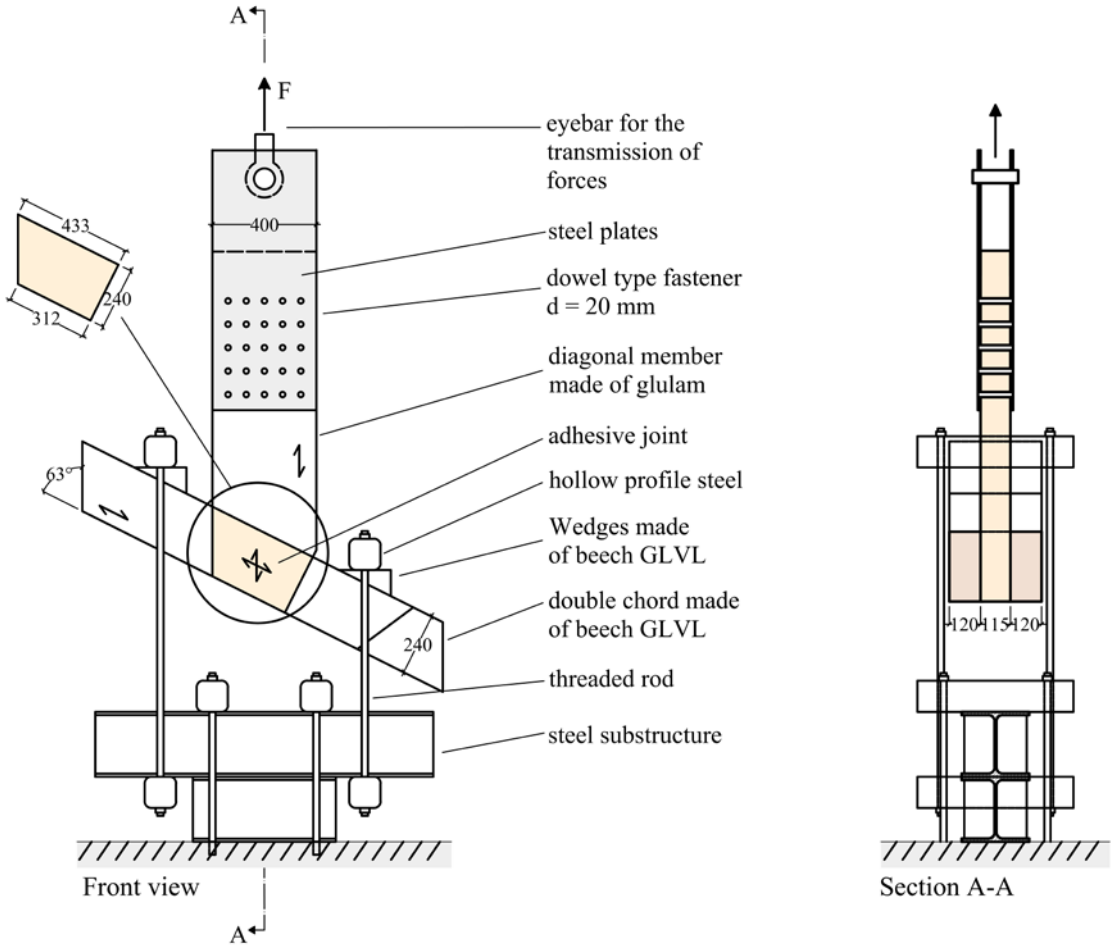

Fig. 1: Scheme and dimensions of experimental set-up for tensile shear test of the investigated truss joint

In order to determine the load/shear capacity of the glued truss joint, the experimental set-up shown in Figs. 1 and 2 for a tensile shear test was used. In this set-up the GLT diagonal member is pulled out in vertical direction parallel to the grain from the double chord of beech GLVL. The tensile load is transferred to the glulam cross-section via two lateral steel plates attached with dowel-type fasteners. The steel plates are connected to the testing machine with a gimballed system consisting of a pin and an eye bar. The support load transfer to the twin chord is performed by steel bars acting on wedge-type beech GLVL fittings. The steel profiles are rigidly connected to the base of the testing machine by threaded rods (see Fig. 2).

The load was applied in a displacement-controlled manner until failure with a hydraulic universal testing machine (max. capacity: F_u=1.6 MN). In addition to the shear strength of the connection, the quality of the bonding was visually assessed at the fracture planes.

Fig. 2: View of realized experimental test set-up for the tension shear tests

3. TEST RESULTS

3.1 Global behavior and failure characteristics

Fig. 3 shows exemplarily load-displacement curves of specimens of four different test series, which can be regarded representative for all investigated specimens. The displacements in Fig. 3 present the stroke of the test machine, hence include additional displacements related to the settling of the dowel-type fasteners in the holes of the steel plates and at the bearing locations of the punctual fixation of the inclined chords.

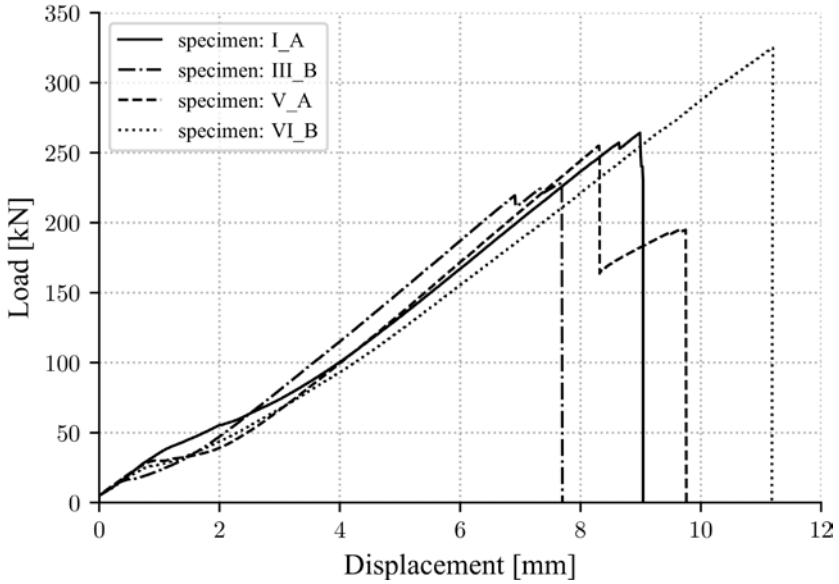

Fig. 3: Exemplary global load-displacement curves of four specimens

Although, the displacements in Fig. 3 are not a direct quantitative measure of the joint stiffness, some general mechanical features of the glued joints can be deduced from the presented curves. Firstly, beyond the initial nonlinear settling of the joint-attachment system the load-displacement behavior of the specimens is highly linear up to sudden pre-peak stiffness discontinuities, if existent, or up to the ultimate load F_u. The pre-peak load drops occurred specimen-dependent in the load range of 90% to 100% of the ultimate load, F_u. For the cases where load recovery beyond the load level of the pre-peak load-drop occurred, no noticeable global stiffness degradation could be observed.

The averaged maximum load F_u per sub-series and the corresponding apparent shear strengths of the entire glued joint are shown in Table 1, computed as $F_{\mathrm{u}}/A_{b,\mathrm{tot}}$, where $A_{b,\mathrm{tot}}$ = 2 · 893 cm^2 = 1786 cm^2 is the total bonded surface (see Fig. 1). The average global shear strength of all joints, with mean values of 1.31 to 1.58 MPa for the individual test series, is relatively low compared to the shear strength of glulam parallel to fiber or rolling shear strength of the beech GLVL (f_v = 3 to 4 MPa), which indicates a decisive effect of strength reducing stress concentrations in the joint.

Table 1: Averaged maximum loads and corresponding global shear strengths of the experiments

Test-series	$F_{u,mean}$ [kN]	$F_{pre\text{-}peak}/F_u$ of specimen i;j [–]	$f_{v,mean}$ [MPa]	n [–]
I	260.5	1.00/0.91	1.46	2
II	241.0	0.92/1.00	1.35	2
III	233.5	0.97/1.00	1.31	2
IV	250.5	1.00/1.00	1.40	2
V	259.0	1.00/1.00	1.45	2
VI	282.5	1.00/1.00	1.58	2

3.2 Bond failure appearance

The specimens failed predominantly due to shear fractures parallel to grain in the spruce glulam close to the glued interface. To a very small extent the failure occurred also in the form of rolling shear in the beech. The fracture planes of one exemplary specimen are shown in Figs. 4a and b, where the predominant failure on the glulam side is evident (lighter color).

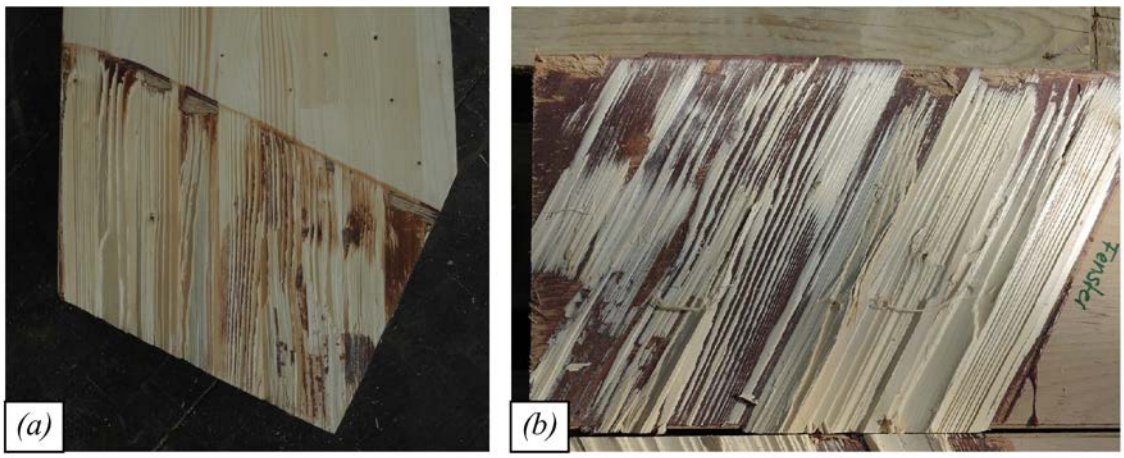

Fig. 4: View of typical fracture planes; (a) fracture appearance on the glulam diagonal; (b) corresponding fracture appearance on the GLVL chord side

4. FINITE ELEMENT MODEL

4.1 Model description

A parametric 3D non-linear finite element (FE) model of the tested configuration, shown in Fig. 5, was created with the commercial software Abaqus v2020 [1] using its Python API. Due to the vertical symmetry of the investigated glued connection only half of the structure was modeled (symmetry along plane *XY*, see

Fig. 5a). Linear brick elements (C3D8) were used to mesh the geometry, with a maximum element size of 10 mm as shown in Fig. 5b. The model was loaded by a vertical displacement on a reference point at the upper end of the vertically positioned GLT member. In order to obtain a uniform distribution of normal stresses while applying the given displacement, an equation constraint was defined between the uppermost nodes (see Fig. 5a) and a reference point according to

$$\sum_{i}^{N} u_{i,3} - N \cdot u_{\mathrm{RP},3} = 0,$$

where $u_{i,3}$ is the vertical displacement of node i, and $u_{\mathrm{RP},3}$ is the vertical displacement of the reference point. This constraint allows for a controlled (stable) path-following during the softening phase, while enabling a uniformly distributed stress situation at the end of the loaded diagonal member. Similar to the experimental set-up, two wedges connected with the chord provide a planar horizontal surface for the support. The structure is supported on single points in the middle of these wedges, which are connected to the top surfaces of the chord by means of so-called “tie” constraints.

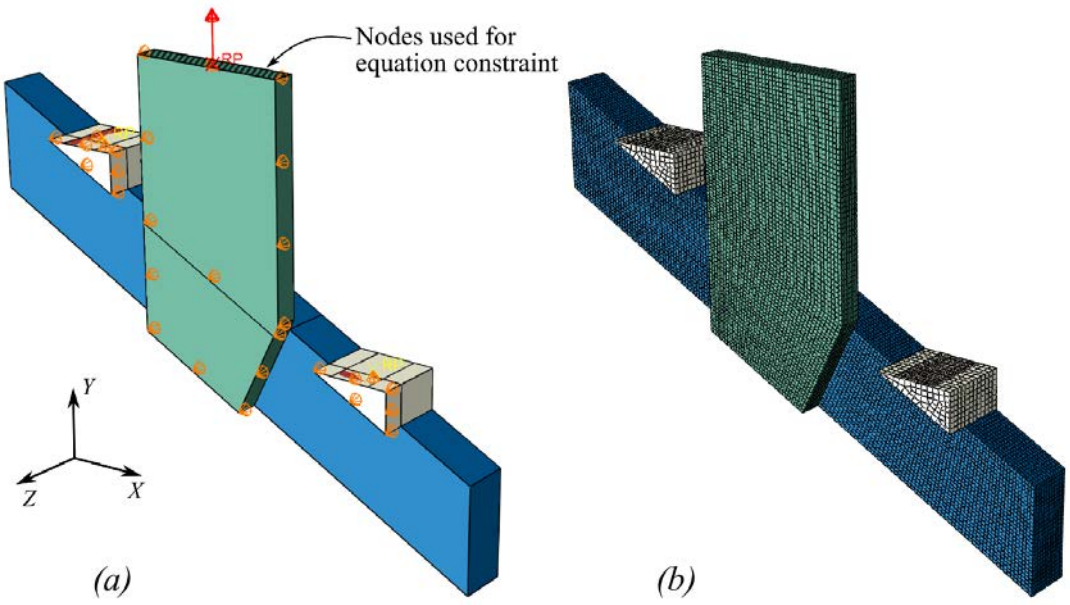

Fig. 5: Finite element model of the investigated bonded truss joint with (a) loading and boundary conditions; (b) mesh

The truss components spruce GLT and beech GLVL were modeled as linear elastic continua. The respective stiffness values and Poisson ratios are given in Table 2. For the modelling of the bonded region between the chord and the diagonal member a cohesive contact behavior with linear energy-based softening was defined. The cohesive contact behavior requires the specification of three stiffness

parameters defined for the direction normal to the surface, k_n, and for both orthogonal shear components, k_{s1} and k_{s2}. The damage initiation is controlled by the maximum nominal stress criterion according to

$$\max\left\{\frac{\sigma_n}{f_n};\frac{\tau_1}{f_{s1}};\frac{\tau_2}{f_{s2}}\right\} \leq 1.$$

The shear strengths f_{s1} and f_{s2} present the minimal strengths of the whole interface in the respective directions. Furthermore, for the damage evolution during softening the fracture energy G_f needs to be specified. The G_f value determines the degree of brittleness/energy dissipation of the failure, and consequently affects possible associated numerical problems during the solution of the system. In order to overcome convergence problems due to the non-linear softening behavior, a damage stabilization can be applied by specifying a viscosity coefficient, ξ. This method considers a viscous regularization which "slows down the rate of increase of damage and increases the fracture energy" [1], therefore caution is needed in order to avoid unrealistic results. In general the viscosity coefficient needs to be a small quantity compared to the characteristic time increment, so that the additional fracture energy will not affect the results [1]. Trial and error is the typical procedure to determine a suitable value for ξ.

Table 2: Stiffness properties of the adherends used in the finite element model

adherend material	E_x [MPa]	E_y [MPa]	E_z [MPa]	ν_{xy} [–]	ν_{xz} [–]	ν_{yz} [–]	G_{xy} [MPa]	G_{xz} [MPa]	G_{yz} [MPa]
beech GLVL	16800	470	470	0.02	0.02	0.2	850	850	85
spruce GLT	11500	300	300	0.02	0.02	0.2	6850	650	65

Different from the rather precisely given and generally acknowledged constitutive parameters for the GLT and GLVL, the quantitative specification of the described cohesive and damage parameters governing the joint capacity and damage evolution is not that straight forward. A parametric analysis was performed in order to analyze the influence of the described cohesive interface and damage behavior parameters. In particular, the influence of the following parameters was investigated: (i) viscosity coefficient (ξ), (ii) material strength (f_s), and (iii) fracture energy (G_f). As starting point the values given by Danielsson and Serrano [4] were used (see Table 3). The specified stiffness parameters of $k_n = k_{s1} = k_{s2}$ = 100 N/mm^2 were kept constant in all investigations reported here.

The values given in [4] are related to the shear failure/damage of an interface between orthogonally oriented laminations of cross laminated timber (CLT). Hence, the shear strengths $f_{s1} = f_{s2}$ in [4] are linked to similar materials on both sides of the joint and an orthogonal arrangement of the layers. In the investigated configuration two very different materials are bonded together at an angle of 63°, influencing the bond strength both due to the material difference and relative fiber orientation. Regarding the influence of the mixture of materials, experience of MPA University of Stuttgart with hybrid joint adherends has evidenced that the interface strength will be improved by the stronger material. Hence, a higher shear strength at least in one direction due to higher rolling shear strength of the beech GLVL needs to be considered.

Table 3: Start values for the parametric study on cohesive parameter influences

	$k_n = k_{s1} = k_{s2}$	f_n	$f_{s1} = f_{s2}$	G_f	ξ
	[MPa]	[MPa]	[MPa]	[Nm/m^2]	[–]
start values [1)]	100	5.0	3.0	1200	10^{-4} [2)]

[1)] According to Danielsson and Serrano [4]; [2)] Value determined by trial

5. CALIBRATION OF COHESIVE INTERFACE PARAMETERS

The parameter calibration was performed by analyzing the impact of the different parameters on the global vertical load-displacement curve of the joint, and comparing it to the experimental results. In order to simplify the analysis, only one parameter was varied at a time, leaving the other (two) parameters fixed as the values by Danielsson and Serrano [4] defined in Table 3. The studied parameters were varied within the ranges shown in Table 4. In the following, the effects of the variation of the viscosity coefficient, local shear strength and fracture energy are briefly discussed.

Table 4: Investigated parameter ranges of the cohesive interface

Parameter	unit	start value	investigated range
Viscocity Coefficient ξ	[–]	10^{-4}	10^{-3} to 10^{-5}
Fracture energy G_f	[Nm/m^2]	1200	600 to 2400
Shear strength $f_{s1} = f_{s2}$	[MPa]	3.0	2.0 to 10.0

5.1 Effect of viscosity coefficient

The viscocity coefficient, ξ, was varied between 10^{-3} and 10^{-5}. Fig. 6a shows the influence of the viscosity parameter on the maximum load capacity and the post-peak load drop behavior. Considering the rather brittle fracture behavior observed in the experiments and illustrated by the experimental load-deflection curves, it can be said that for viscosity coefficients $\xi \leq 10^{-4}$ the FE-results mirror the real measured brittle behavior of the specimens with sufficient accuracy. Values of $\xi \gg 10^{-4}$ result not only in a less abrupt descent of the load, but also produce an increase in maximum load, as revealed in the graph for $\xi = 10^{-3}$, being a result of the artificially increased fracture energy. Since these effects are undesired, as they do not relate to the experimental observations and theoretical expectations, a value of $\xi = 10^{-4}$ was considered sufficient for ensuring the convergence of the model without noticeably affecting the results. Therefore, ξ=10^{-4} was chosen for all parameter studies on the effect of local shear strength and fracture energy presented below.

5.2 Effect of local shear strength

The impact of the local shear strength of the adjoining elements on the joint capacity within the investigated range of $f_{s1} = f_{s2} = 2$ to 10 N/mm^2 (G_f = const. = 1200 Nm/m^2 and ξ = const. = 10^{-4}) is shown in Fig. 6b. Ultimate load of the joint increases with rising f_s-values from 204 kN to 242 kN, i.e. by about 20%. Excluding the rather unrealistic pure softwood rolling shear strength of 3 to 4 MPa renders the shear strength influence to a rather negligible quantity. So, for f_s = 4 to 10 MPa, the capacity increases by maximally 6%. Considering the apparent small impact of the local shear strength beyond obviously too low values (e.g. 2 MPa) on the maximum load, it is concluded for the time being, that the influence of the differences between the rolling shear strength of the beech GLVL and shear strength of glulam is not influencing the joint capacity in very pronounced manner. The exact influence and related small scale experimental tests are subject of ongoing investigations.

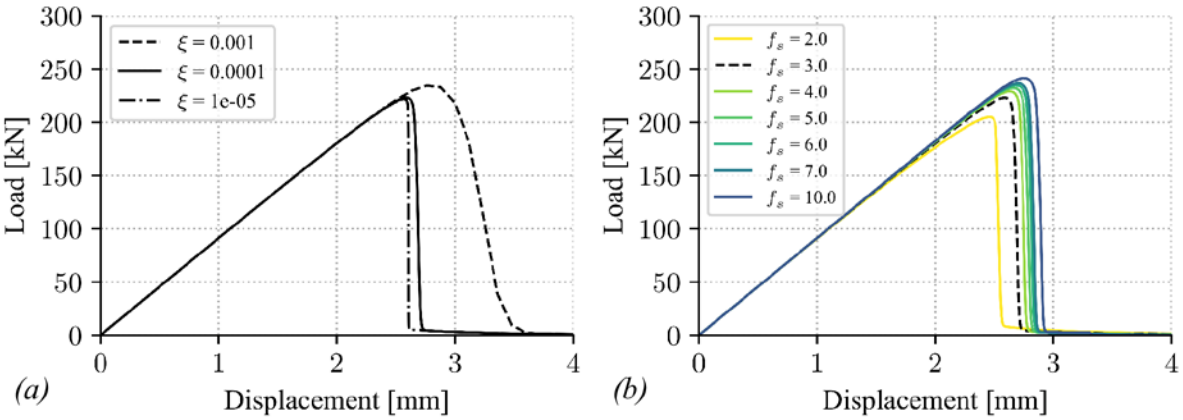

Fig. 6: Global load displacement curve at constant fracture energy G_f = 1200 Nm/m2 dependent on (a) viscosity coefficient (f_s = const.= 3 MPa); (b) interface shear strength ($\xi = 10^{-4}$)

5.3 Effect of fracture energy

Results of the fracture energy variations on the joint capacity are presented in Fig. 7. Respective numerical results are given in Table 5. It is apparent and plausible that the increase of fracture energy leads to a significant increase of the maximum joint capacity. The physical reason for this feature consists in the fact that all bond areas having experienced local failure are still contributing significantly to load uptake during softening, i.e. during their gradually reducing resistance on their descending strength path. So, stress homogeneity in the total joint area increases significantly with raising G_f values. The increase of fracture energy from 600 Nm/m^2 to 2400 Nm/m^2, i.e. by a factor of four leads to a joint capacity increase by a factor of 1.81, i.e. from 163 kN to 295 kN. It is further evident that the rate of capacity gains reduces with higher fracture energies, which would apply to a fully plastic material law, too.

Fracture energies ranging from 1200 Nm/m^2 to 2400 Nm/m^2 deliver computational joint capacities, which cover almost the whole range of test results (compare Table 1 and Fig. 7). The determination of appropriate fracture energies can of course be performed, as done here, by inverse calibration, but from a material science point of view it should be a direct result from testing of the intrinsic material property. Most substantial work in this field has been performed by Wernersson [20], [21], Wernersson and Gustafsson [22], [23] however exclusively aiming at shear parallel and tension perpendicular to grain of softwoods. Further work is needed for hybrid softwood-hardwood timber interfaces and various angles to grain.

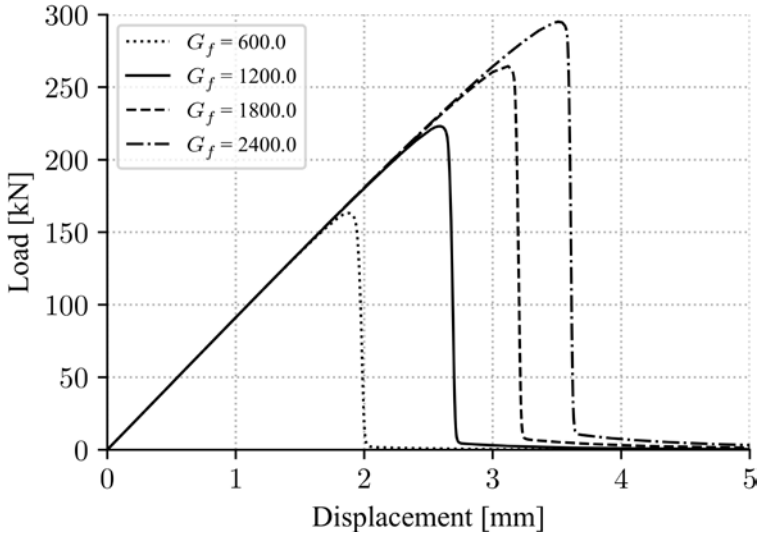

Fig. 7: Effect of interface fracture energy on global load-displacement curve and ultimate loads (constant shear strength f_s = 3.0 MPa and viscosity coefficient $\xi = 10^{-4}$)

Table 5: Ultimate loads and apparent shear strengths dependent on interface fracture energy

G_f [Nm/m^2]	F_u [kN]	f_v [MPa]
600	163.2	0.91
1200	223.1	1.25
1800	264.4	1.48
2400	295.1	1.65

6. DAMAGE LOCALIZATION AND EVOLUTION

The cohesive interface approach allows for the identification of the localization and for the quantification of the initiation and spacial evolution of the damage, illustrated briefly in this and the next chapter. In this chapter the complex damage/fracture evolution of the bonded interface is shown in rather qualitative manner. Quantitative stress distributions are given below. In both cases, qualitative and quantitative description, the joint damage and stress status is revealed for the elastic state, here chosen as $0.95F_u$, for ultimate load F_u being already influenced significantly by the localized non-linear interface behavior and at the post-peak softening branch at $0.7F_u$. As the non-linear analysis is based on the displacement increments, then resulting in forces and stresses, Table 6 specifies the applied displacement values, too. Fig. 8 shows the mentioned load/displacement steps used for the damage progress description within the total bonded joint area, revealed in

Fig. 8b as shaded area. The paths shown in Fig. 8b are related to the quantitative stress discussion below. Path 1 marks the begin of the joint where the spruce diagonal firstly meets the beech chords at a fiber angle of 63°; Path 3 is located at mid-length of the joint.

Fig. 9 shows the localization of the fracture and then the spacial evolution at the mentioned discrete displacement/load steps. The graphs reveal the Abaqus contact status plots differentiating between the states: bonded, sticking, slipping and not in contact, i.e. fractured. The comparison of Fig. 9a and b illustrates the bond area fracture on-set, located at the protruding chord-diagonal corner. The revealed location of the fracture on-set is bound to the vicinity of a geometric discontinuity leading to a high stress concentration. This can be deduced from linear FEM-analysis, too, yet without any decisive hints on possible fracture progression and the load level. Fig. 9c highlights the bond area fracture state at the very steep, almost unstable load displacement path, resulting from the quasi brittle interface. Additionally Fig. 9d shows the almost final fracture state related to a minorly increased applied displacement of 2.76 mm (vs. 2.71 mm).

The computation-based graphs confirm intuitive thinking on the force and the interface shear stress transfer between the chords and the diagonal(s). This means that the bondline capacity is at higher load levels primarily retained in a bond area where the (shear) stress flow is not disturbed by geometry discontinuities.

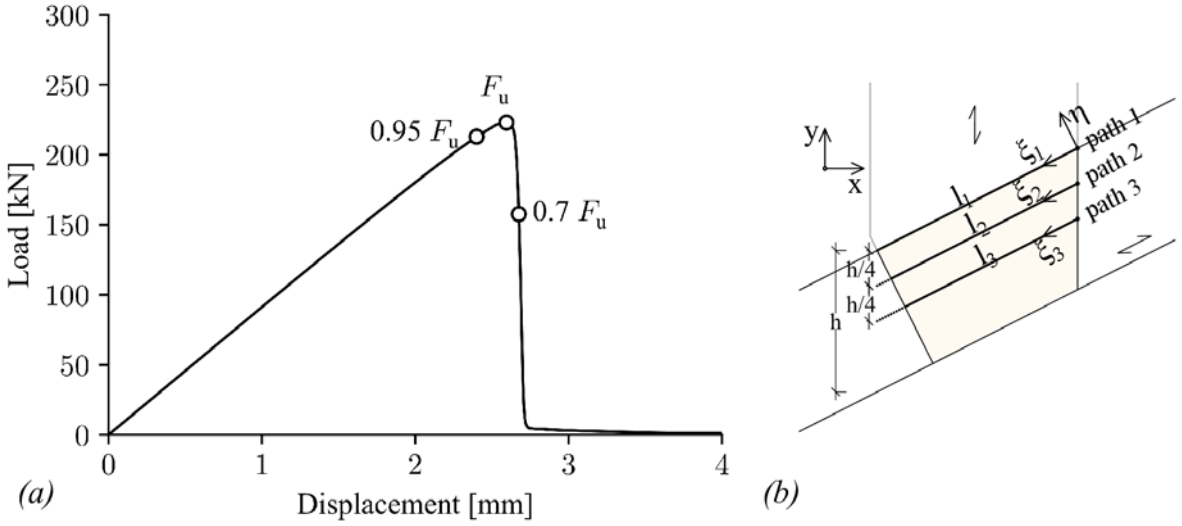

Fig. 8: Illustration of load levels and geometry locations for damage and shear stress distributions in Figs. 9 to 11 (a) used global load-deflection points (b) used geometry paths

Table 6: Applied displacements and corresponding loads and load levels

Applied displacement u_{RP3} [mm]	corresponding load F [kN]	Load level F/F_u [–]
2.40	213.0	0.95
2.60	223.1	1.0
2.68	157.6	0.7

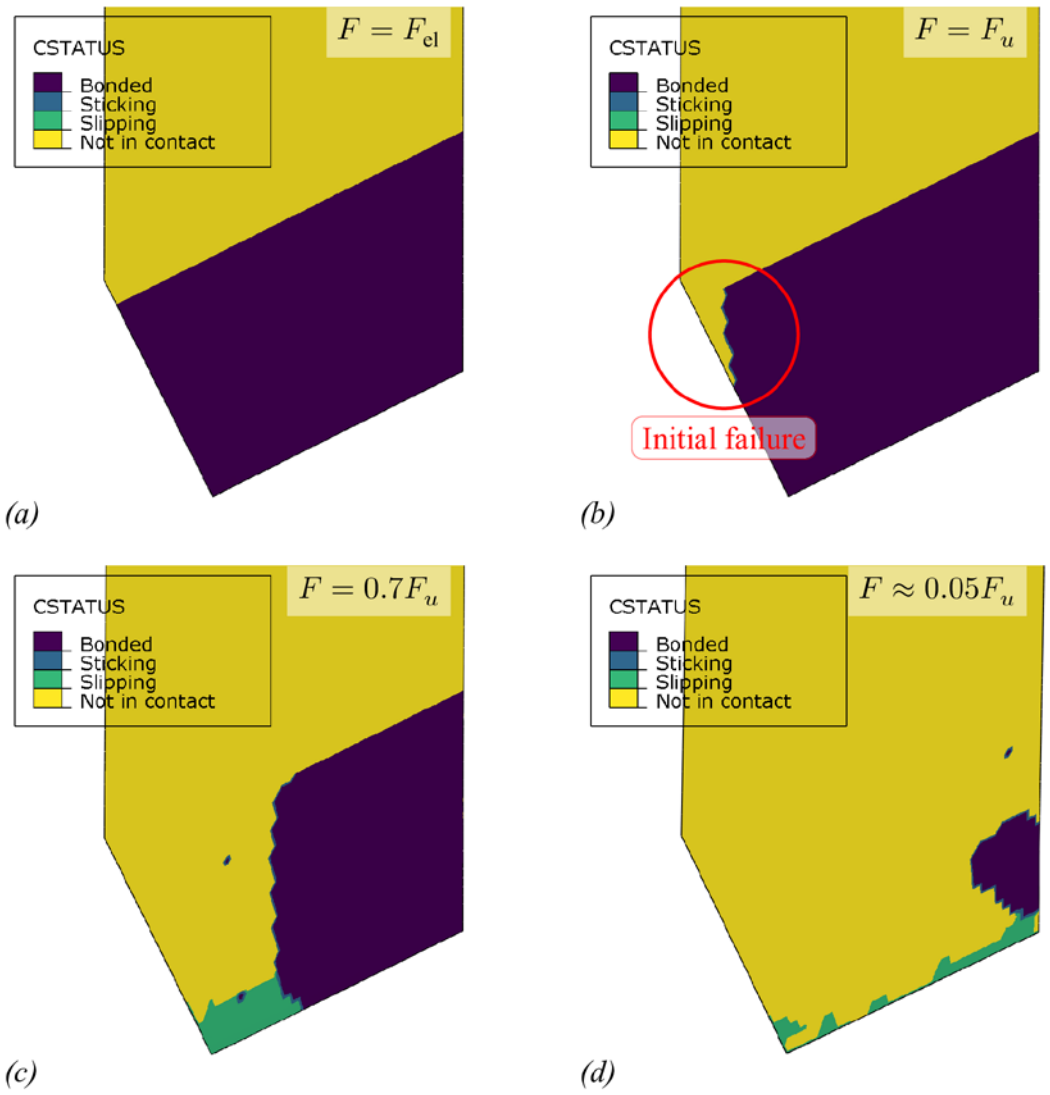

Fig. 9: Spacial interface fracture evolution steps of the investigated bonded truss joint at different pre and post peak load steps (a) elastic state at $0.95F_u$, applied displacement 2.40 mm; (b) ultimate load state, incorporating initial damage at protruding corner area, applied displacement 2.64 mm; (c) progressed damage state at $0.7F_u$, applied displacement 2.71 mm; (d) visualization of massive damage extension as compared to Fig. 9c; applied displacement 2.76 mm

6.1 Stress distribution at progressing damage

In quantitative complementation on the above sketched spacial damage evolution in the total joint area, shear stresses are depicted in Figs. 10 and 11 at selected paths 1 to 3 shown in Fig. 8b. In detail the interface adjacent shear stresses in both adherends, beech GLVL and spruce GLT are considered at two relevant coordinate directions, η and y, Figs. 10 and 11, respectively. Direction η represents for the beech GLVL the local on-axis rolling shear direction perpendicular to fiber orientation, whereas the y-axis coincides with the direction parallel to fiber of the spruce GLT. Similar as for the spacial damage evolution, the shear stresses are given for the three selected load levels of 0.95, 1.0 and 0.70 of the maximum load F_u. Figs. 10a–d depict the shear stresses τ_η at the elastic (0.95 F_u), peak (F_u) and post-peak (0.70 F_u) state along paths 1 and 3 for both adherends, beech GLVL and spruce GLT. Note: for origin of coordinates ξ_1 and ξ_2 along length of the respective paths see Fig. 8b.

All four graphs reveal at 0.95 F_u and F_u rather prevailingly (except Fig. 10a) pronounced shear stress peaks at both ends of paths 1 and 3, with very similar stress distributions.

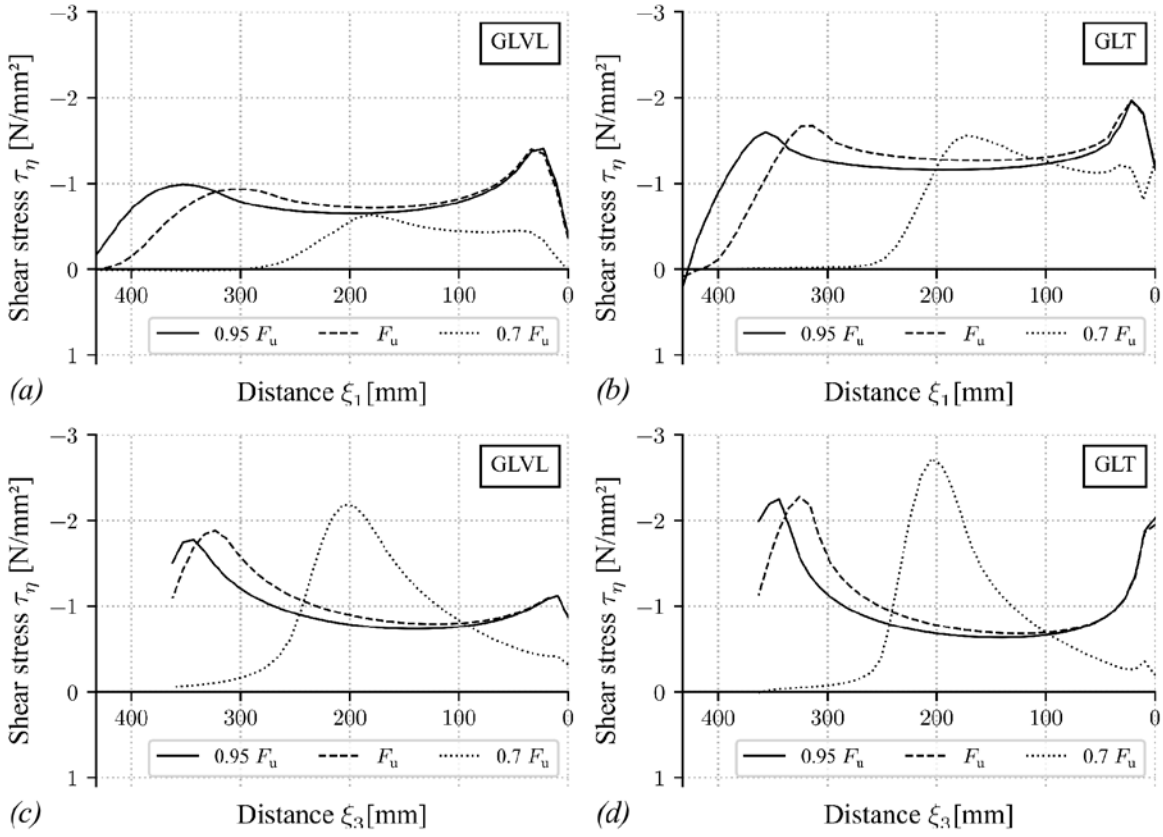

Fig. 10: Shear forces τ_η along Path 1 in (a) beech chord and (b) spruce diagonal; and along Path 3 in (c) beech chord and (d) spruce diagonal

The initiated damage process between (0.95 – 1.0) F_u along path 1 can be clearly deduced from Figs. 10a and b by the shift of the shear stresses away from the protruding joint corner at $\xi_1/\ell_1 \approx 1$ towards the inner part of the joint ($\xi_1/\ell_1 < 1$). At path 3 this damage initiation and stress shift is also existent, yet less expressed as in case of path 1. The described differences of the shear stress along the two selected paths in the small load increment from 0.95 F_u to F_u is exactly mirroring the spacial damage evolution depicted in Figs. 9a and b.

The shear stress distributions at load level 0.7 F_u, i.e. at the descending branch of the joint load capacity, differ significantly, as can be expected, from the shapes at the elastic and peak load state. At both paths 1 and 3, and for both adherend materials, the stresses are practically zero for $\xi_i/\ell_i \geq 0.6\ to\ 0.7$, then followed by a marked stress increase with evident differences between path 1 and 3. At path 1 the shear stresses increase in both adherends, GLVL and GLT, roughly to the F_u level and then decrease and remain roughly constant. Very different from the stress evolution at path 1, the stress shape at path 3 resembles somewhat a Gaussian function, i.e. presents a pronounced stress peak at about mid-width of the joint ($\xi_3/\ell_3 \approx 0.4\ to\ 0.6$). Furthermore, the stress level exceeds the peak stresses at F_u (located at a different position at about $\xi_3/\ell_3 \approx 1.0$) by factors of about 1.16 - 1.19. The stress distributions along path 3 reveal that the damage progression has shifted the stress uptake in the joint area towards the center right part of the joint ($\xi_3/\ell_3 \lesssim 0.5$). This feature is fully in line with the further progression of the cohesive status from 0.7 F_u to $F_u \sim 0$ shown in Figs. 9c and d.

Finally, the quantitative differences of the shape-wise well conforming interface shear stresses in the GLVL and the GLT are regarded. Along path 1 the stress levels of both adherends differ significantly. Disregarding the stress peaks, the mean shear stress level at 0.95 F_u and F_u in GLT is very roughly 80% higher as compared to the GLVL. At the load level of 0.7 F_u this difference is even more pronounced and denoted by factor of two. At path 3 the mentioned stress level differences are much less expressed and primarily confined to the peak stresses where the GLT shear stresses are roughly 20% higher.

The shear stresses τ_y, i.e. in direction parallel to fiber of the spruce GLT, depicted in Fig. 11, resemble shape-wise closely the distributions shown in Fig. 10 for coordinate direction ξ. This is also true for the stress levels for both materials in the case of path 3, so at mid-length of the joint. Contrary, at path 1 the shear stresses in the GLVL and the GLT are more / rather different at all load levels, 0.95 F_u,

F_u, 0.7 F_u, and the peak stresses are much higher, i.e. rougly by a factor of 1.6 at ($\xi_3/l_3 \approx$ 0.8).

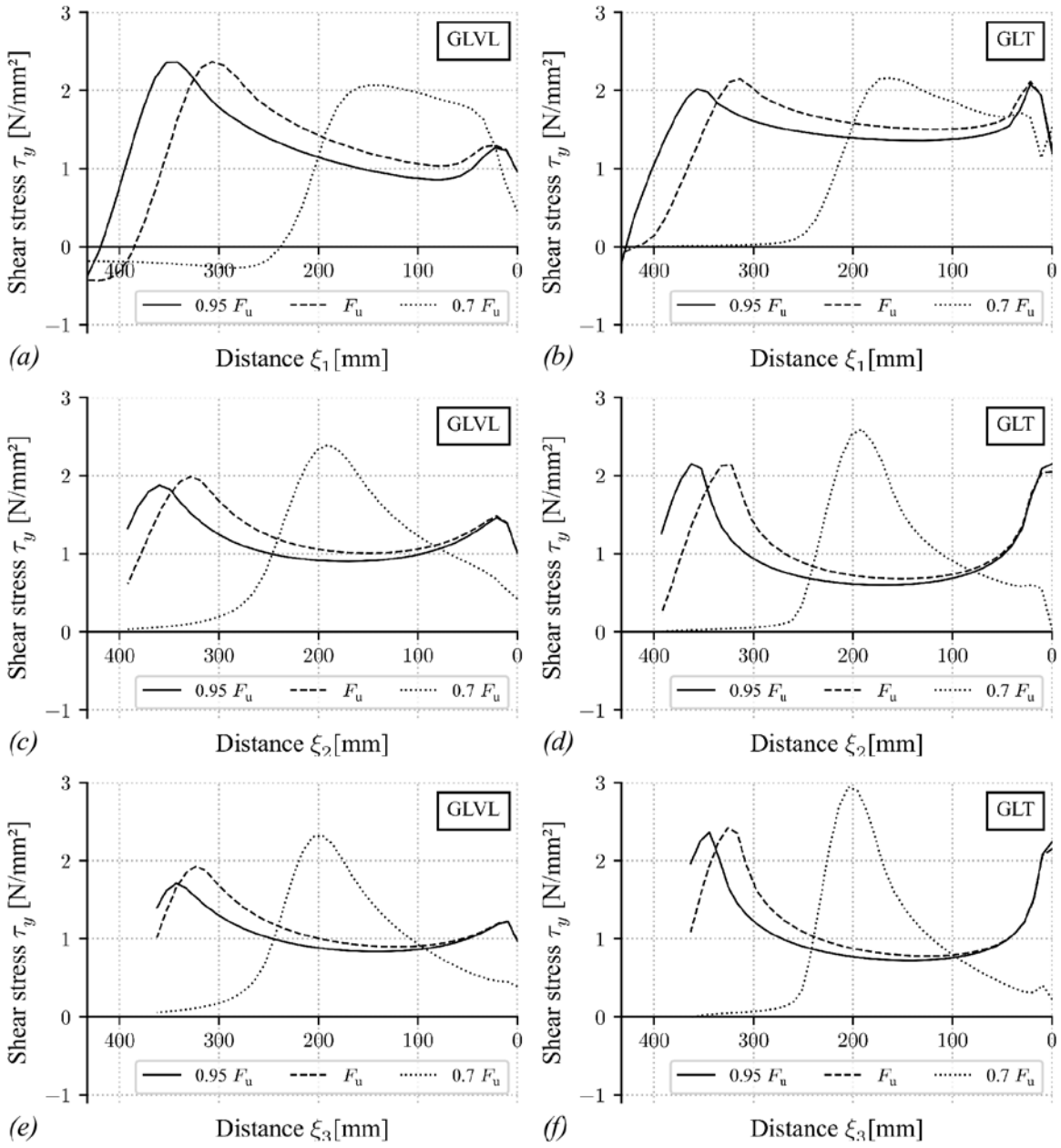

Fig. 11: Shear forces τ_y (i.e. parallel to fiber in spruce diagonal) along Path 1 in (a) beech chord and (b) spruce diagonal; along Path 2 in (c) beech chord and (d) spruce diagonal; and along Path 3 in (e) beech chord and (f) spruce diagonal

7. DISCUSSION

The FEM calculations revealed high load-capacity detrimental effects of geometric discontinuities located at the borderline between the jointed components and especially at a protruding corner of the trapezoidal-shaped bond area. These discontinuities lead to high stress concentrations and induce failure initiation. The progressive softening of the bond/interface area leads to a stress redistribution

towards the inner part of the joint area. However the non-linear effects are too small to create substantial capacity gains and hence global failure as predicted by FEM analysis is quasi brittle what corresponds well to the fracture behavior seen in the experiments.

The comparatively low apparent global shear strength of the experiments results from the averaged distribution of the ultimate load over the entire bond area. This crude engineering approach does not consider the damage-relevant stress concentrations. The results of the FE-analysis provide a fairly good estimation of the experimental load capacities. However, the determination of the cohesive interface parameters, here derived from literature and inverse calibrations, deserves more work.

8. CONCLUSIONS

The developed parametric FE model, including cohesive behavior with fracture softening in the adherend interface, supports full scale experimental data and enables the further optimization of the investigated glued truss joint. This will be followed up via variations of geometry, sizes and adherend materials altogether with closer investigations on the interface parameters. Finally, the shear capacity of the optimized configuration resulting from the latter parametric analysis has to be validated by further experimental tests.

ACKNOWLEDGEMENTS

The reported research was partially supported by company Brüninghoff Holz GmbH & Co. KG, Heiden. Further, the partial support by the Deutsche Forschungsgemeinschaft (DFG, German Research Foundation) under Germany's Excellence Strategy – EXC 2120/1 – 390831618 is gratefully acknowledged.

REFERENCES

[1] ABAQUS: *ABAQUS/Standard user's manual, version 2020*, Providence, RI, USA : Dassault Systèmes, 2020

[2] AICHER, S.: *Investigations on glued structural timber-steel plate joints*. In: *Otto-Graf-Journal* Vol. 2 (1991). Stuttgart, Germany, FMPA Baden-Württemberg (Otto-Graf-Institute), pp. 8–36

[3] AICHER, S., KLÖCK, W.: *Reliability based analysis of glued lap joint resistance*. In: PRO 22: Proceedings of the International RILEM Symposium – Joints in timber structures. Stuttgart, Germany: RILEM publications S.A.R.L, 2001, pp. 473–482

[4] DANIELSSON, H., SERRANO, E.: *Cross laminated timber at in-plane shear loading – strength and fracture analysis of shear mode III*. In: Proceedings of the World Conference on Timber Engineering (WCTE 2021). Santiago, Chile, 2021

[5] DIEHL, F., WENKER, J.L., BLETZ-MÜHLDORFER, O., BATHON, L., SCHUFF, M., SIEVERDINGBECK, K., SCHNEERMANN, J.: *Hybrid-Leichtbauträger für weitgespannte Hallentragwerke, final research report:* FNR Verbundforschungsvorhaben Förderkennzeichen 22023017/22007818, 2021

[6] EN 13377: *Prefabricated timber formwork beams – Requirements, classification and assessment*, Brussels, Belgium : European Committee for Standardization, 2002

[7] EN 14080: *Timber structures – Glued laminated timber and glued solid timber - requirements*, Brussels, Belgium : European Committee for Standardization, 2013

[8] EN 301: *Adhesives, phenolic and aminoplastic, for load-bearing timber structures — Classification and performance requirements*, Brussels, Belgium : European Committee for Standardization, 2013

[9] ETA-14/0354: *Glued laminated timber made of hardwood – Structural laminated veneer lumber made of beech*, Vienna, Austria : Austrian Institute of Construction Engineering, 2018

[10] GLOS, P., HORSTMANN, H.: *Design of glued joints*. In: Proceedings of international timber engineering conference. vol. 3. London, United Kingdom, 1991, pp. 3.77–3.84

[11] HANDEL, P.: *Konstruktionsgrundsätze und Bemessungstabellen für den Dreieck-Streben-Bau*, Berlin : Verlag von Wilhelm Ernst & Sohn, 1977

[12] JOHANSSON, C.-J.: *Limträramar med förband av inlimmade stalstänger*. SP Report 1992:60: Swedish National Testing Institute, 1992

[13] KEMMSIES, M.: *The influence if adhesives and bonding techniques on the properties of glued timber-steelplates joints*. SP Report 1994:39: Swedish National Testing Institute, 1994

[14] PALM, J.: *Limträramar skarvade med inlimmade plattstänger av stal - experimentell och teoretisk undersökning*. SP Report 1991:67: Building Technology, Swedish National Testing Institute, 1991

[15] SERRANO, E.: *Adhesive joints in timber engineering – modeling and testing of fracture properties*. Report TVSM-1012, Lund, Sweden: Division of Structural Mechanics, Lund University, 2000

[16] SERRANO, E., GUSTAFSSON, P.J.: *Modelling and testing of adhesive joints in timber engineering*. In: *PRO 22:* Proceedings of the International RILEM Symposium – Joints in Timber Structures, 2001, pp. 463–472

[17] SIGMUND, O.: *Topology optimization: A tool for the tailoring of structures and materials*. In: THOMPSON, J. M. T. (ed.) Philosophical Transactions of the Royal Society of London. Series A: Mathematical, Physical and Engineering Sciences vol. 358, The Royal Society (2000), Nr. 1765, pp. 211–227. doi: 10.1098/rsta.2000.0528

[18] TANNERT, T.: *Probabilic design of adhesively bonded timber joints* (in German). In: Bautechnik 87 (2010), Nr. 10, pp. 623–629

[19] VALLÉE, T., TANNERT, T., HEHL, S.: *Experimental and numerical investigations on full-scale adhesively bonded timber trusses*. In: Materials and Structures 44 (2011), pp. 1745–1758. doi: 10.1617/s11527-011-9735-8

[20] WERNERSSON, H.: *Wood Adhesive Bonds – Fracture Softening Properties in Shear and in Tension*. Report TVSM-3012, Lund, Sweden : Division of Structural Mechanics, Lund University, 1990

[21] WERNERSSON, H.: *Fracture Characterization of Wood Adhesive Joints*. Report TVSM-1006, Lund, Sweden : Division of Structural Mechanics, Lund University, 1994

[22] WERNERSSON, H., GUSTAFSSON, P.J.: *The complete stress-slip curve of wood-adhesives in pure shear*. In: Mechanical behaviour of adhesive joints. Paris, France, Edition Pluralis Paris (1987), pp. 139–150

[23] WERNERSSON, H., GUSTAFSSON, P.J.: *Strength and constitutive properties of adhesive joints*. In: Proceedings of International Conference on Timber Engineering. vol. 1, 1988, pp. 673–582

[24] YANG, H., CROCETTI, R., LARSSON, G., GUSTAFSSON, P.J.: *Experimental study on innovative connections for large span timber truss structures*. In: Proceedings of the IASS Working Groups 12 + 18 International Colloquium 2015: International Association for Shell; Spatial Structures (IASS), 2015